Supporting Information

Single-Crystal NMR Characterization of Halogen Bonds

Yijue Xu, Bulat Gabidullin, and David L. Bryce*

*Author to whom correspondence is to be addressed

Department of Chemistry and Biomolecular Sciences

University of Ottawa

10 Marie Curie Private

Ottawa, Ontario K1N 6N5

Canada

Tel: +1-613-562-5800 ext.2018; fax: +613-562-5170

Email: dbryce@uottawa.ca

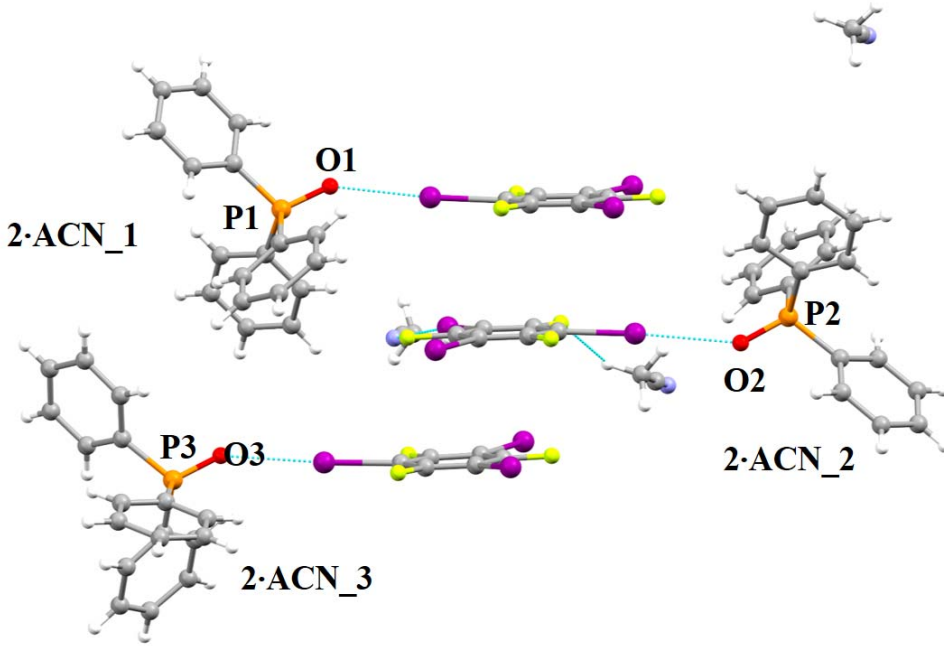

Figure S1. Halogen bond geometry in one unit cell of cocrystal **2·ACN** from single-crystal X-ray diffraction. The three crystallographically distinct sites are shown with labels consistent with the main text. Molecules **2·ACN _1** and **_3** share similar environments and orientation whereas **2·ACN _2** faces in the opposite direction.

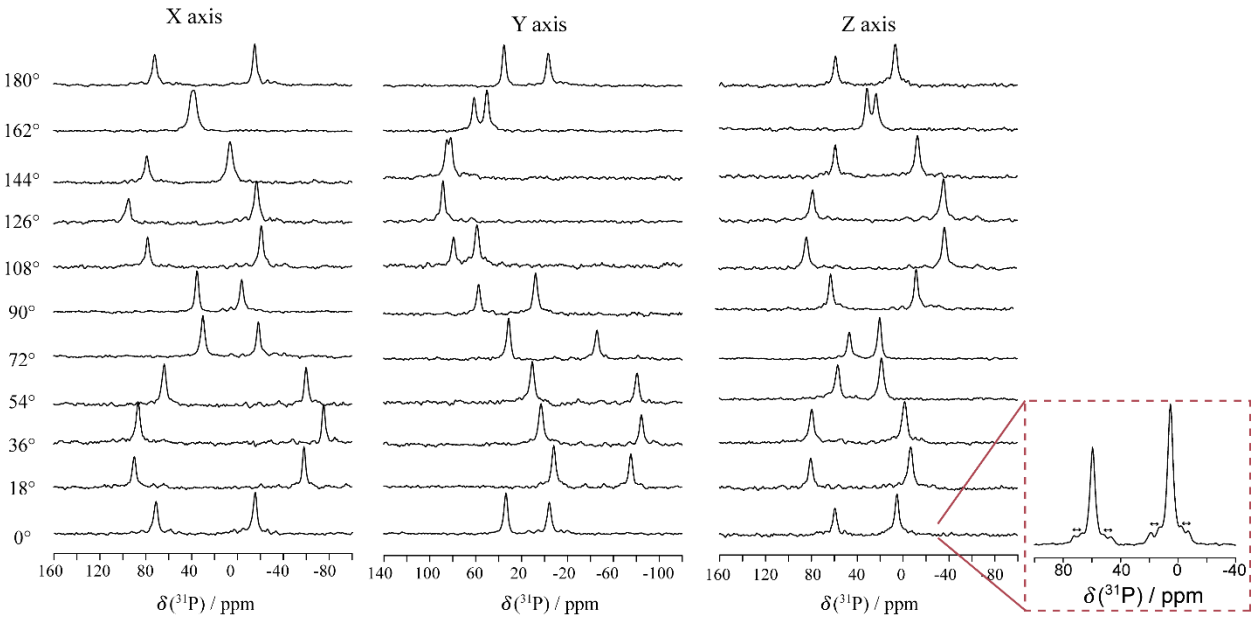

Figure S2. Single-crystal ^{31}P NMR spectra (B_0 = 9.4 T) for $Ph_3P^{17}O$. Spectra were obtained at 9° rotational increments about the X, Y, and Z axes. Here only every second spectrum is shown. Shown in the inset is a magnification of the spectra to show the presence of spin-spin coupling between ^{17}O and ^{31}P.

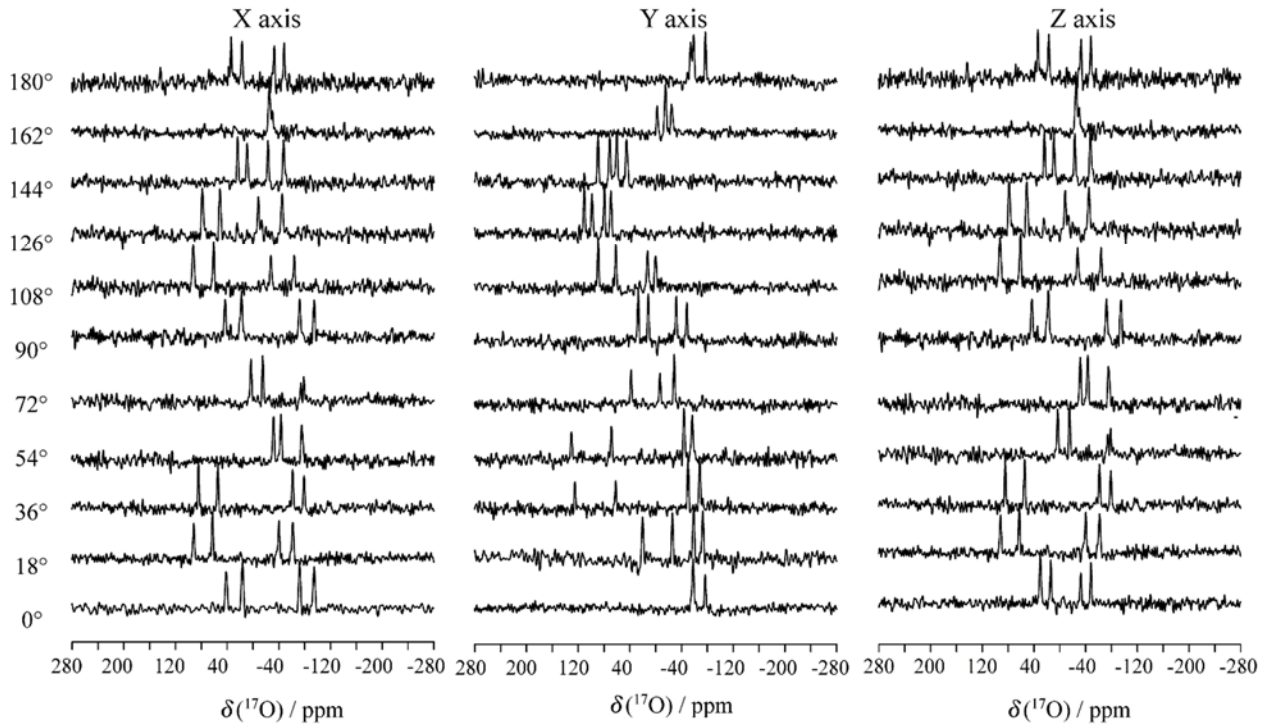

Figure S3. Single-crystal ^{17}O NMR spectra (B_0 = 9.4 T) for monoclinic $Ph_3P^{17}O$. Spectra were obtained at 9° rotational increments about the X, Y, and Z axes. Here only every second spectrum is shown.

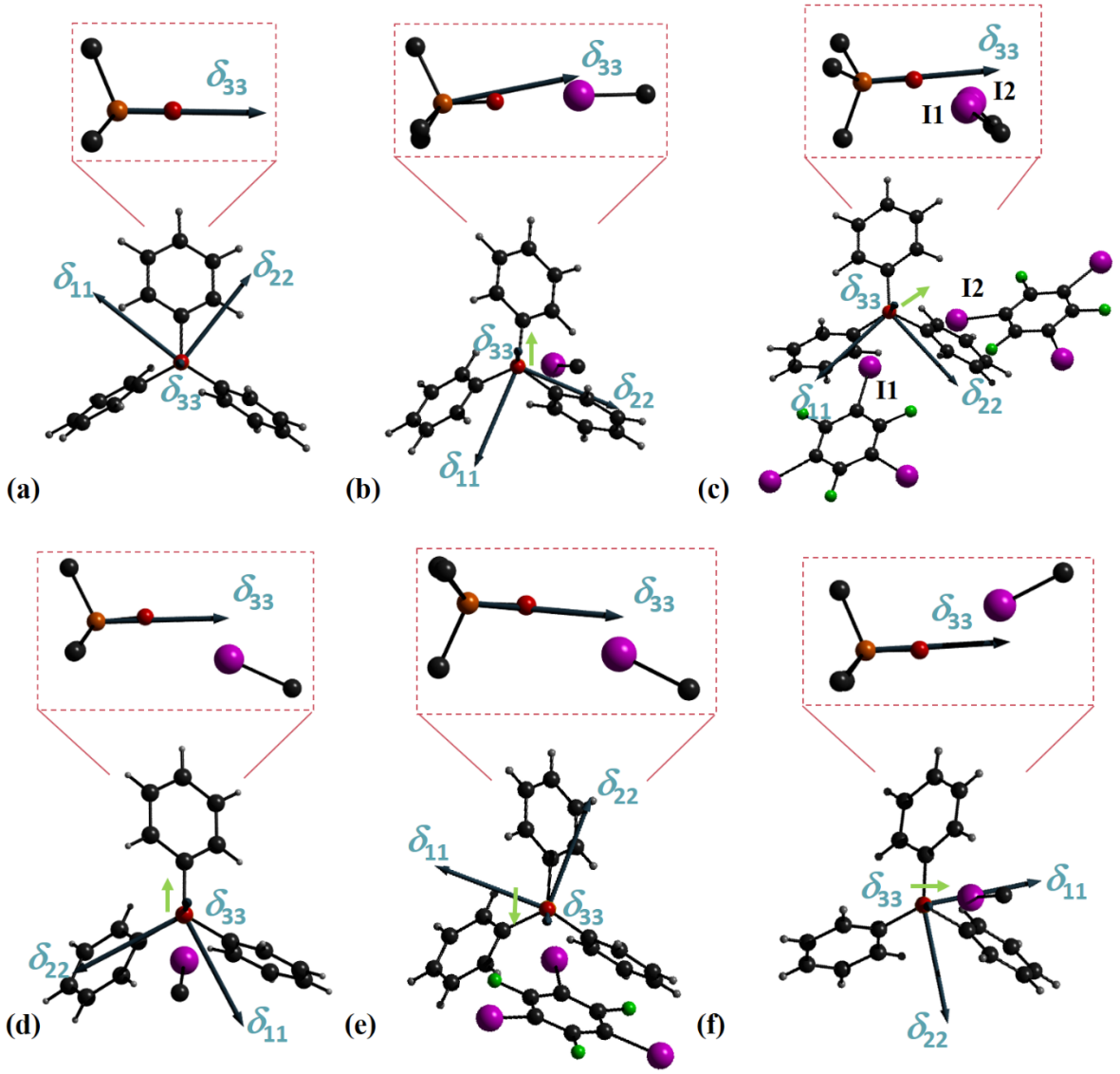

Figure S4. Depictions of the crystal structure of the starting material $Ph_3P^{17}O$ (a), and its halogen-bonded cocrystals: **1** (b), **2** (c) and **2·ACN_1** (d), **2·ACN_2** (e) and **2·ACN_3** (f) where the P=O bond is perpendicular to the plane for illustration of the orientation of ^{31}P CS tensors (indicated by dark green arrows) in the molecular frame. The light green arrows indicate the direction of δ_{33} movement upon halogen bond formation. In **1**, **2·ACN_1**, and **2·ACN_3**, only iodine-carbon fragments are shown; the rest of the molecules are omitted to more clearly show the vectors. Shown in the insets are the truncated projections of the structures when the P=O bond is within the plane to illustrate the change in direction of δ_{33}.

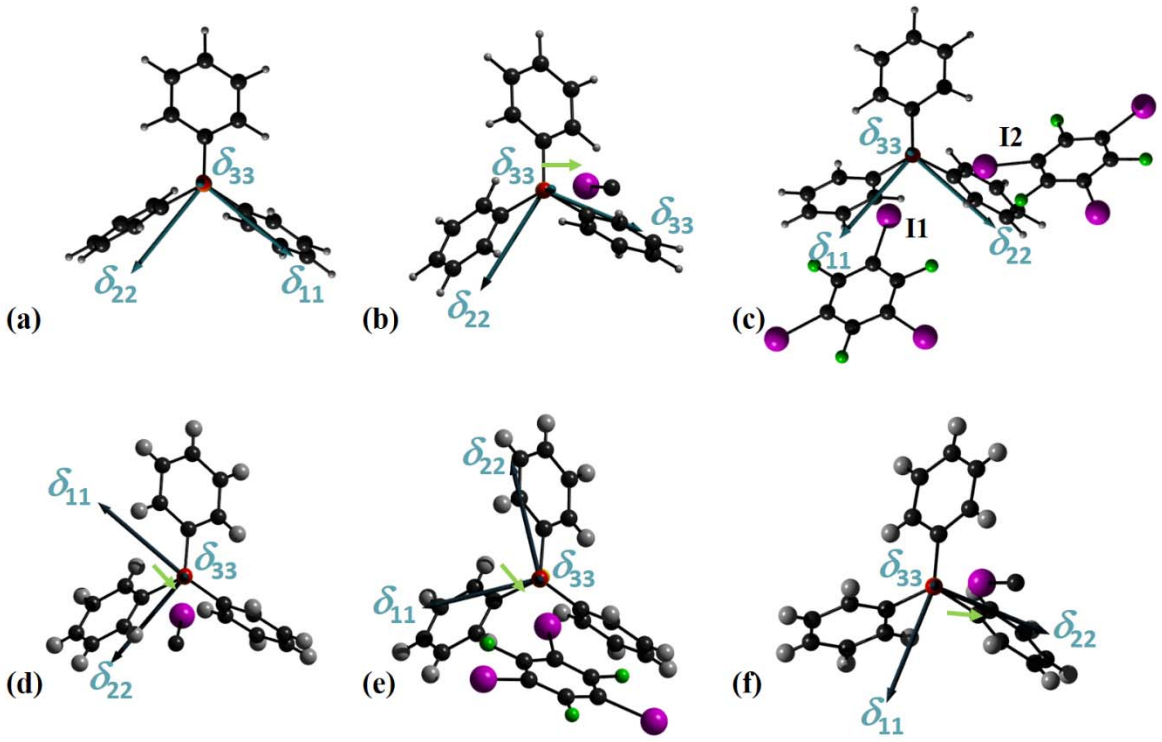

Figure S5. Projection of the crystal structures of the starting material $Ph_3P^{17}O$ (a), and its halogen-bonded cocrystals: **1** (b), **2** (c), and **2·ACN _1** (d), **2·ACN _2** (e) and **2·ACN _3** (f) where the P=O bond is perpendicular to the plane for illustration of the GIPAW DFT-calculated orientations of ^{31}P the CS tensors (indicated as dark green arrows) in the molecular frame. The light green arrows indicate the direction of δ_{33} movement upon halogen bonding. In **1**, **2·ACN _1**, and **2·ACN _3**, only iodine-carbon fragments are shown and the rest of the molecules are omitted to more clearly show the vectors.

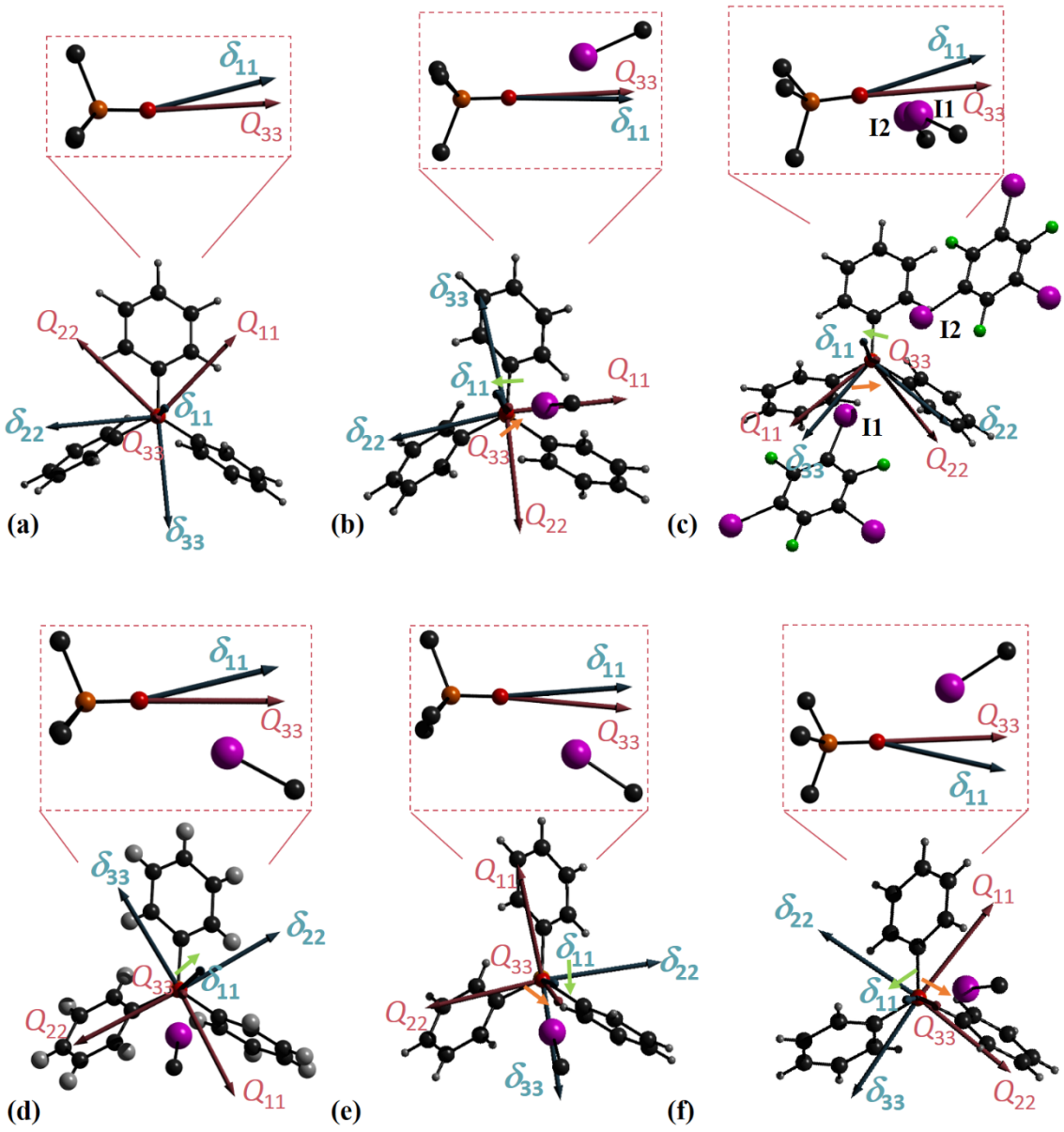

Figure S6. Projection of the crystal structure of the starting material $Ph_3P^{17}O$ (a), and its halogen-bonded cocrystals: **1** (b), **2** (c) and **2·ACN_1** (d), **2·ACN_2** (e), and **2·ACN_3** (f) where the P=O bond is perpendicular to the plane to illustrate the orientation of the principal components of the ^{17}O CS (dark green arrows) and quadrupolar coupling tensors (pink arrows) in the molecular frame. The light green arrows and orange arrows, respectively, indicate the direction of δ_{11} and Q_{33} movement upon halogen bonding. In **1** and **2·ACN**, only iodine-carbon fragments are shown and

the rest of the molecules are omitted to more clearly show the vectors. Shown in the insets are the simplified projections of the structures when the P=O bond is within the plane to illustrate the change of the direction of δ_{11} and Q_{33}.

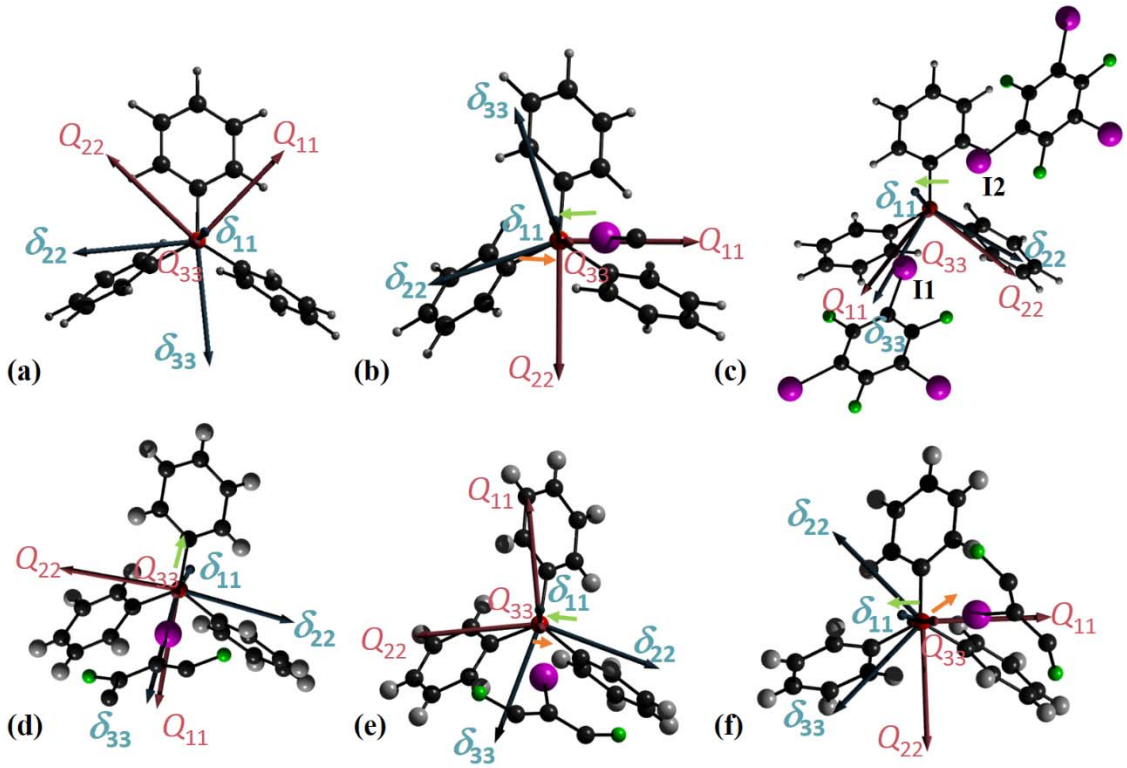

Figure S7. Projection of the crystal structure of the starting material $Ph_3P^{17}O$ (a), and its halogen-bonded cocrystals: **1** (b), **2** (c) and **2·ACN_1** (d), **2·ACN _2** (e), and **2·ACN _3** (f) where the P=O bond is perpendicular to the plane to illustrate the GIPAW DFT-calculated orientation of the principal components of ^{17}O CS (dark green arrows) and quadrupolar coupling tensors (pink arrows) in the molecular frame. The green arrows and orange arrows, respectively, indicate the

direction of δ_{11} and Q_{33} movement upon halogen bonding. In **1** and **2·ACN**, only iodine-carbon fragments are shown and the rest of the molecules are omitted to more clearly show the vectors.

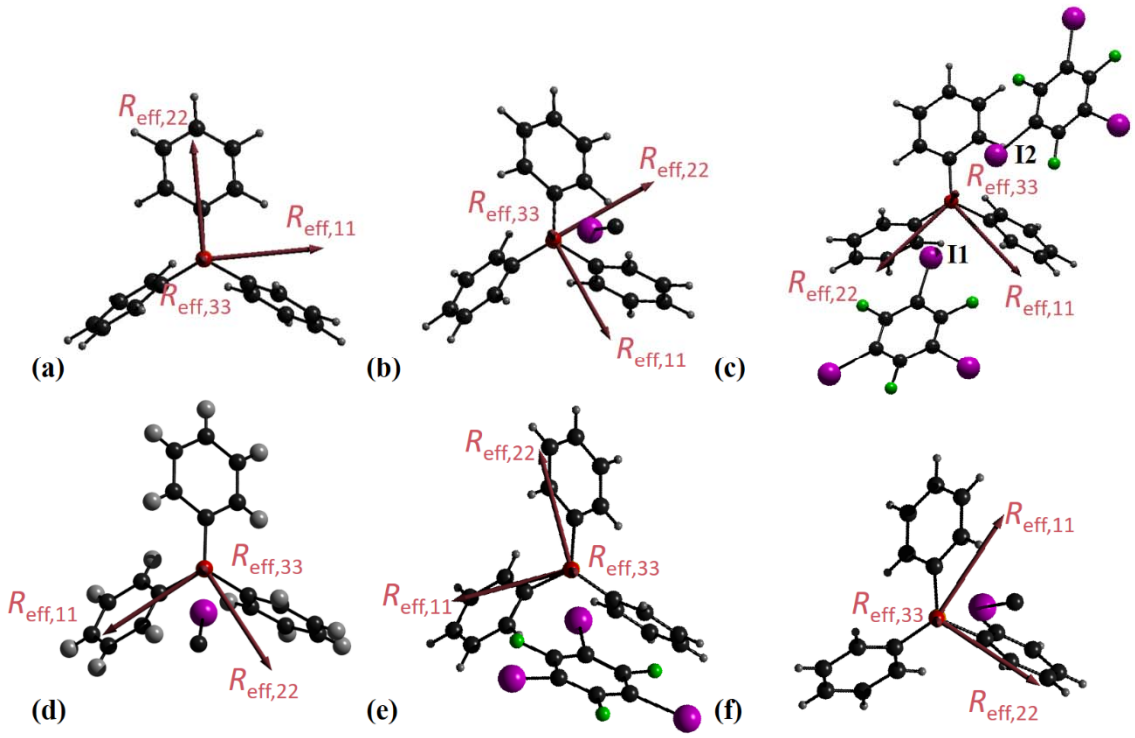

Figure S8. Projection of the crystal structures of the starting material $Ph_3P^{17}O$ (a), and its halogen-bonded cocrystals: **1** (b), **2** (c) and **2·ACN _1** (d), **2·ACN _2** (e), and **2·ACN _3** (f) where the P=O bond is perpendicular to the plane for illustration of the experimental orientations of ^{31}P-^{17}O effective dipolar coupling principal components (indicated as pink arrows) in the molecular frame. In **1**, **2·ACN _1**, and **2·ACN _3**, only iodine-carbon fragments are shown and the rest of the molecules are omitted to more clearly show the vectors.

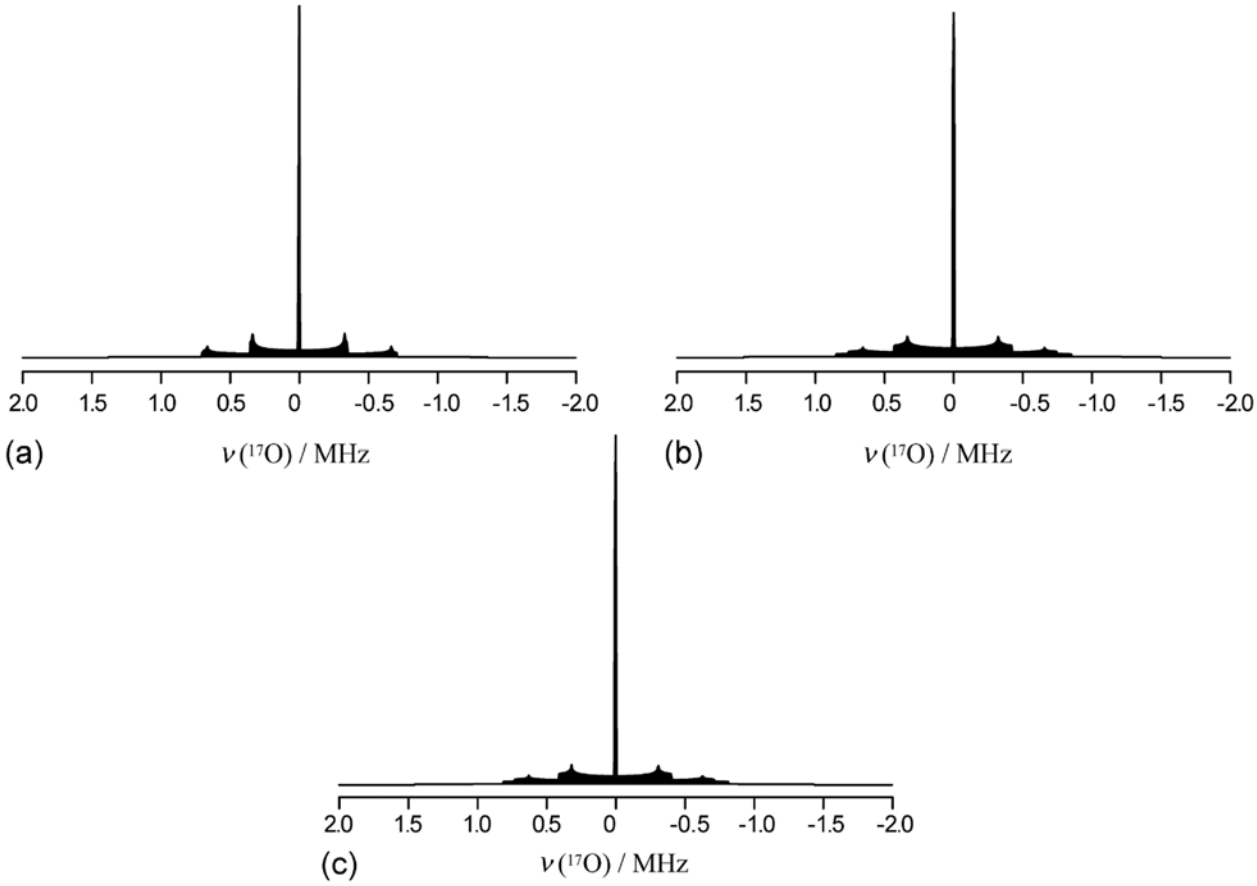

Figure S9. Simulated ^{17}O static powder NMR spectra at 9.4 T for Ph_3PO (a) and its halogen-bonded cocrystals **1**(b) and **2**(c). The relatively low intensities make the measurement of STs by single-crystal NMR very challenging.

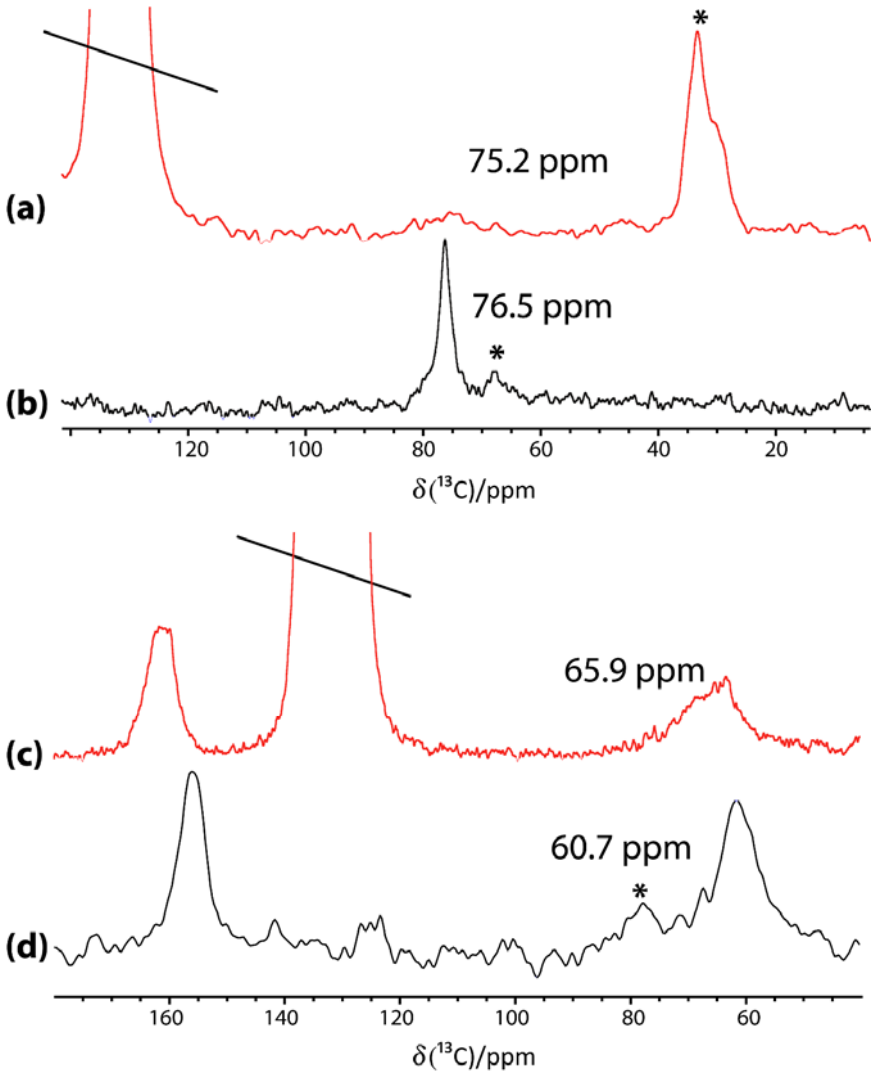

Figure S10. Experimental ^{13}C MAS SSNMR spectra for the region of the carbon covalently bonded to iodine. The spectra corresponding to the starting materials *p*-$C_6F_4I_2$(b) and *sym*-$C_6F_3I_3$(d) are shown in black; the spectra corresponding to the cocrystals **1**(a) and **2**(c) are shown in red. The spectra of cocrystals **1** and **2** were obtained using ^{13}C cross-polarization (CP) experiments with a MAS rate of 10 kHz whereas the spectrum of *sym*-$C_6F_3I_3$(d) was obtained using a ^{13}C Hahn-echo (i.e., $\pi/2-\tau_1-\pi-\tau_2-$acq) experiment with spinning speed of 8 kHz. The spectrum of *p*-$C_6F_4I_2$ (b) was acquired at 21.1 T and was previously shown in reference 1. Other spectra were acquired at 9.4 T. The asterisks indicate spinning sidebands.

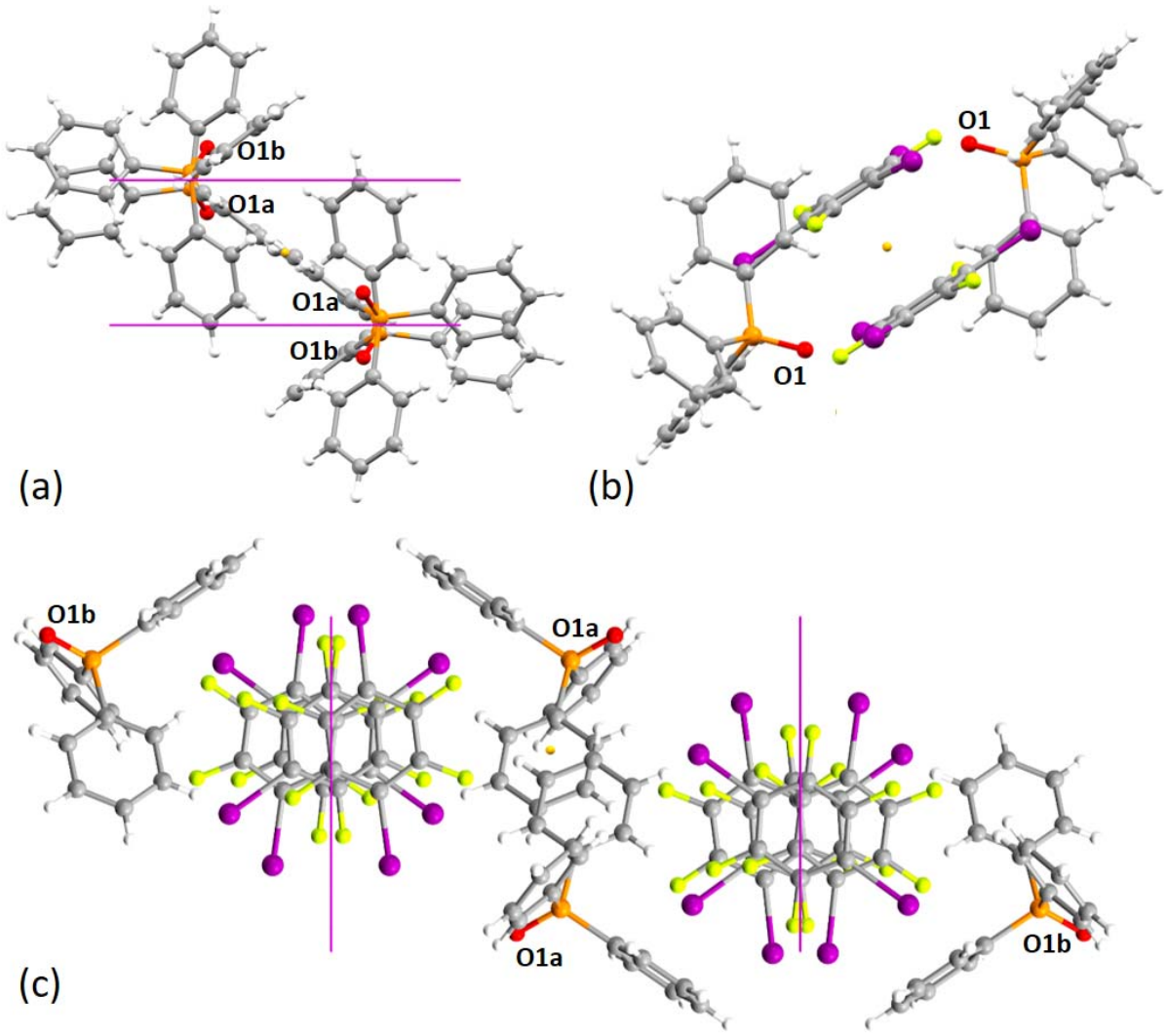

Figure S11. Representation of one unit cell of Ph_3PO (a) and its halogen-bonded cocrystal **2**(b) and **1**(c) from single-crystal X-ray diffraction. The small yellow-orange spheres indicate the inversion centers, resulting in two magnetically equivalent oxygen atoms represented by the same label. The pink lines indicate glide planes, generating two magnetically non-equivalent oxygen atoms represented by different letters.

Table S1. Single-Crystal X-Ray Data and Selected Data Collection Parameters for **2·ACN** (cif 1907250)

	2·ACN
Empirical Formula	$C_{26}H_{18}F_3I_3NOP$
Formula Weight	829.08
Crystal Size, mm^3	0.722 × 0.404 × 0.353
Crystal System	Triclinic
Space Group	$P\bar{1}$
Z	6
Volume, Å	4229.61(13)
Calculated density, Mg m^{-3}	1.953
a, Å	13.6994 (2)
b, Å	18.2829 (4)
c, Å	20.3552 (3)
α, deg	115.9880 (10)
β, deg	92.9510 (10)
γ, deg	108.6840 (10)
Absorption coefficient, mm^{-1}	3.421
F(000)	2340
θ range for data collection, °	1.845 to 26.500
Limiting indices	$-15 \le h \le 17$, $-22 \le k \le 18$, $-24 \le l \le 25$
Reflections collected/ unique	33791 / 17404
R_{int}	0.0298
Completeness to $\theta = 25.242°$, %	99.3
Max and min transmission	0.746 and 0.534
Data/ restraints/ parameters	17404 / 0 / 949
Goodness-of-fit on F^2	0.975
Final *R* indices [$I > 2\alpha(I)$]	$R_1 = 0.0427$, $wR_2 = 0.0904$
R indices (all data)	$R_1 = 0.0983$, $wR_2 = 0.1179$
largest diff. peak and hole, e·$Å^{-3}$	0.669 and -1.145

Table S2. Principal Components and Direction Cosines of the ^{31}P Chemical Shift Tensors in the Crystal Axis Frame[a]

compound		components / ppm	a*	b	c
	δ_{11}	96.6(3)	-0.60(2)	0.53(1)	0.60(2)
Ph_3PO	δ_{22}	83.3(6)	0.74(1)	0.65(2)	0.16(4)
	δ_{33}	-101.3(7)	0.31(4)	-0.54(2)	0.79(1)
	δ_{11}	93.9(1)	0.06(3)	-0.48(3)	0.88(3)
1	δ_{22}	89.1(7)	0.90(2)	-0.35(3)	-0.25(5)
	δ_{33}	-92.0(2)	0.42(4)	0.81(3)	0.41(1)
	δ_{11}	96.4(3)	0.10(3)	-0.95(3)	0.31(2)
2[b]	δ_{22}	82.5(7)	-0.96(2)	-0.01(3)	0.28(5)
	δ_{33}	-92.0(7)	0.26(4)	0.32(3)	0.91(1)
2·ACN	δ_{11}	92 (1)	-0.93(2)	0.37(5)	0.07(1)
	δ_{22}	87(2)	-0.37(4)	-0.83(2)	-0.43(2)
	δ_{33}	-94(6)	0.10(2)	0.42(3)	-0.90(1)
	δ_{11}	93(1)	-0.98(2)	-0.10(1)	-0.17(1)
	δ_{22}	87(2)	-0.16(2)	0.92(2)	0.37(2)
	δ_{33}	-96(6)	0.12(2)	0.39(3)	-0.91(1)
	δ_{11}	92(1)	-0.92(2)	0.38(5)	0.06(1)
	δ_{22}	87(2)	-0.37(4)	-0.83(2)	-0.42(2)
	δ_{33}	-98(6)	0.11(2)	0.41(3)	-0.90(2)

[a] The convention used for designating the three principal components of the CS tensor is $\delta_{11} \geq \delta_{22} \geq \delta_{33}$.

[b] Compound **2** cannot provide error estimates generated from comparison between two crystallographic equivalent but magnetically distinct sites like Ph_3PO and **1**. Uncertainties from single-crystal NMR data fitting are only on the order of 0.1 ppm. Therefore, we estimate the error to be similar to the largest error present in analysis of Ph_3PO and **1**.

Table S3. Principal Components and Direction Cosines of the ^{17}O Chemical Shift Tensors in the Crystal Axis Frame[a]

compound		components / ppm	a*	b	c
Ph_3PO	δ_{11}	151(8)	-0.43(2)	0.41(3)	-0.81(1)
	δ_{22}	12(1)	-0.86(2)	0.05(5)	0.49(3)
	δ_{33}	-8(2)	0.24(3)	0.91(2)	0.33(6)
1	δ_{11}	109(3)	-0.50(5)	-0.71(3)	-0.49(1)
	δ_{22}	19(2)	0.63(7)	0.08(7)	-0.78(7)
	δ_{33}	5(1)	0.59(6)	-0.70(3)	0.40(12)
2[b]	δ_{11}	152(8)	0.42(5)	0.29(3)	0.86(1)
	δ_{22}	33(2)	0.90(7)	-0.23(7)	-0.37(7)
	δ_{33}	-10(2)	-0.09(6)	-0.93(3)	0.36(12)
2·ACN[b]	δ_{11}	125(8)	0.19(5)	0.56(3)	-0.81(1)
	δ_{22}	29(2)	-0.92(7)	0.38(7)	0.05(7)
	δ_{33}	-11(2)	-0.34(6)	-0.74(3)	-0.58(12)
	δ_{11}	133(8)	0.33(5)	0.57(3)	-0.75(1)
	δ_{22}	41(2)	-0.89(7)	-0.08(7)	-0.46(7)
	δ_{33}	-30(2)	0.32(6)	-0.82(3)	-0.47(12)

[a] The convention used for designating the three principal components of the CS tensor is $\delta_{11} \geq \delta_{22} \geq \delta_{33}$.

[b] Compounds **2** and **2·ACN** cannot provide error estimates generated from comparison between two crystallographic equivalent but magnetically distinct sites like Ph_3PO and **1**. Uncertainties from single-crystal NMR data fitting are only on the order of 0.1 ppm for CS tensors. Therefore, we estimate the error to be similar to the largest error present in analysis of Ph_3PO and **1**.

Table S4. Principal Components (in MHz) and Direction Cosines of the ^{17}O Quadrupolar Coupling Tensors in the Crystal Axis Frame[a]

compound		components / MHz	a*	b	c
Ph_3PO	Q_{33}	-0.228(2)	0.32(2)	-0.50(2)	0.80(1)
	Q_{22}	0.118(1)	0.22(6)	-0.78(2)	-0.58(1)
	Q_{11}	0.110(3)	-0.92(2)	-0.37(6)	-0.14(2)
1	Q_{33}	-0.248(1)	0.46(3)	0.80(1)	0.37(1)
	Q_{22}	0.130(2)	-0.72(1)	0.58(2)	-0.37(4)
	Q_{11}	0.118(1)	-0.51(3)	-0.10(1)	0.85(1)
2[b]	Q_{33}	-0.240(2)	0.20(3)	0.28(2)	0.94(1)
	Q_{22}	0.132(1)	0.98(6)	0.01(2)	-0.21(4)
	Q_{11}	0.108(3)	0.06(3)	-0.96(6)	0.27(2)
2·ACN[b]	Q_{33}	-0.247(2)	0.11(3)	0.43(2)	-0.90(1)
	Q_{22}	0.135(1)	0.89(6)	-0.44(2)	-0.10(4)
	Q_{11}	0.112(3)	-0.43(3)	-0.79(6)	-0.43(2)
	Q_{33}	-0.241(2)	0.13(3)	0.44(2)	-0.89(1)
	Q_{22}	0.133(1)	-0.97(6)	-0.13(2)	-0.21(4)
	Q_{11}	0.107(3)	-0.21(3)	0.89(6)	0.40(2)

[a] The convention used for designating the three principal components of the quadrupolar coupling tensor is $|Q_{33}| \geq |Q_{22}| \geq |Q_{11}|$.

[b] Compounds **2** and **2·ACN** cannot provide error values estimated from comparison between two crystallographic equivalent but magnetically distinct sites like Ph_3PO and **1**. Uncertainties from single-crystal NMR data fitting are only on the order of 0.001 MHz for EFG tensors. Therefore, we estimate the error to be similar to the largest error present in analysis of Ph_3PO and **1**.

Table S5. Principal Components (in Hz) and Direction Cosines of the Averaged Effective ^{17}O-^{31}P Dipolar Coupling Tensors in the Crystal Axis Frame[a]

compound		components / Hz	a*	b	c
Ph_3PO	$R_{eff,33}$	3715(42)	-0.33(3)	0.51(2)	-0.80(1)
	$R_{eff,22}$	-1832(32)	0.22(11)	0.86(2)	0.46(4)
	$R_{eff,11}$	-1883(10)	-0.92(3)	0.03(11)	0.39(4)
1	$R_{eff,33}$	3734(20)	-0.45(3)	-0.80(3)	-0.40(2)
	$R_{eff,22}$	-1821(10)	0.74(2)	-0.09(5)	-0.67(3)
	$R_{eff,11}$	-1913(30)	-0.50(5)	0.59(3)	-0.63(2)
2[b]	$R_{eff,33}$	3795(42)	0.26(3)	0.32(3)	0.91(3)
	$R_{eff,22}$	-1853(32)	0.10(11)	-0.95(5)	0.31(4)
	$R_{eff,11}$	-1942(30)	-0.96(5)	-0.01(11)	0.28(4)
2·ACN[b]	$R_{eff,33}$	3883(42)	0.11(3)	0.46(3)	-0.88(3)
	$R_{eff,22}$	-1870(32)	-0.44(11)	-0.77(5)	-0.46(4)
	$R_{eff,11}$	-2014(30)	0.89(5)	-0.44(11)	-0.12(4)
	$R_{eff,33}$	3944(42)	0.12(3)	0.44(3)	-0.89(3)
	$R_{eff,22}$	-1900(32)	-0.30(11)	0.87(5)	0.39(4)
	$R_{eff,11}$	-2044(30)	-0.95(5)	-0.22(11)	-0.23(4)

[a] The convention used for designating the three principal components of the effective ^{31}P-^{17}O dipolar coupling tensor is $|R_{eff,33}| \geq |R_{eff,11}| \geq |R_{eff,22}|$.

[b] Compounds **2** and **2·ACN** cannot provide error values estimated from comparison between two crystallographic equivalent but magnetically distinct sites like Ph_3PO and **1**. Uncertainties from single-crystal NMR data fitting are only on the order of 10 Hz. Therefore, we estimate the error to be similar to the largest error present in analysis of Ph_3PO and **1**.

Reference:

(1) Viger-Gravel, J.; Leclerc, S.; Korobkov, I.; Bryce, D. L. Correlation Between ^{13}C Chemical Shifts and the Halogen Bonding Environment in a Series of Solid *para*-Diiodotetrafluorobenzene Complexes. *CrystEngComm* **2013**, *15*, 3168–3177.